Protection against Atmospheric Corrosion of Zinc in Marine Environment Rich in H2S Using Self-Assembled Monolayers Based on Sargassum fluitans III Extract

Prescilla Lambert, Mahado Said-Ahmed, Benoit Lescop, Stéphane Rioual, Mounim Lebrini

coatings

MDPI

Article

Protection against Atmospheric Corrosion of Zinc in Marine Environment Rich in H_2S Using Self-Assembled Monolayers Based on *Sargassum fluitans III* Extract

Prescilla Lambert [1], Mahado Said-Ahmed [1], Benoit Lescop [2], Stéphane Rioual [2] and Mounim Lebrini [1,*]

[1] Laboratory of Materials and Molecules in Aggressive Media, UR 4_1 Université des Antilles, UFR Sciences Technologies Environment, 97233 Schoelcher, France; prescilla.lambert@etu.univ-antilles.fr (P.L.); mahado.saidahmed@univ-antilles.fr (M.S.-A.)

[2] Laboratoire des Sciences et Techniques de l'Information de la Communication et de la Connaissance, CNRS, UMR 6285, Brest University, 29200 Brest, France; benoit.lescop@univ-brest.fr (B.L.); stephane.rioual@univ-brest.fr (S.R.)

* Correspondence: mounim.lebrini@univ-antilles.fr; Tel.: +33-594-29-75-14; Fax: +33-594-28-47-86

Abstract: The self-assembled monolayers (SAMs) process is one of the techniques used for the production of ultra-thin layers. The present work is therefore devoted to the study of the inhibition of zinc corrosion in a marine environment rich in H_2S by SAMs based on *Sargassum fluitans III*. The protective effect of crude extracts of *Sargassum fluitans* on the surface of zinc using the SAMs process was evaluated by gravimetry and impedance on two different sites after three months of exposure. The formation of SAMs was characterized by FTIR, and the corrosion products formed on the surfaces were analyzed by XRD. The results obtained show that SAMs based on *Sargassum fluitans III* effectively inhibit zinc corrosion.

Keywords: corrosion; marine environment; zinc; SAMs; *Sargassum fluitans III*; EIS; DRX

Citation: Lambert, P.; Said-Ahmed, M.; Lescop, B.; Rioual, S.; Lebrini, M. Protection against Atmospheric Corrosion of Zinc in Marine Environment Rich in H_2S Using Self-Assembled Monolayers Based on *Sargassum fluitans III* Extract. *Coatings* **2024**, *14*, 988. https://doi.org/10.3390/coatings14080988

Academic Editor: Chi Tat Kwok

Received: 11 June 2024
Revised: 16 July 2024
Accepted: 2 August 2024
Published: 5 August 2024

1. Introduction

Corrosion is an insidious phenomenon known to cause a great deal of damage (material, environmental, etc.). The atmosphere plays a key role in these physicochemical phenomena. Parameters such as humidity, heat, and salinity come into play. The marine environment is the perfect illustration of a naturally aggressive environment for most materials. Few metals can withstand it, which is why they need to be protected. Zinc is widely used as a coating to protect metals from corrosion, particularly for galvanizing ferrous metallic products. Zinc corrosion has been extensively studied in various atmospheres, including marine environments rich in H_2S. These studies have shown that zinc corrosion is closely linked to environmental conditions such as humidity and temperature, as well as the chemical composition of the atmosphere, whether it is enriched with corrosive pollutants or not [1–3]. Typically, in the presence of a marine atmosphere, zinc corrosion primarily leads to the formation of simonkolleite ($Zn_5Cl_2(OH)_8{\cdot}H_2O$) and gordaite ($NaZn_4(SO_4)(OH)_6Cl{\cdot}6H_2O$). However, a previous study has shown that in a marine atmosphere rich in H_2S, [4] this surface composition is altered. Zinc sulfide (ZnS) and elemental sulfur are the predominant products. The presence of H_2S alters the corrosion process, leading to acceleration of the corrosion kinetics. In order to combat corrosion, several studies have been conducted to investigate the corrosion resistance of metals immersed in a corrosive solution containing inhibitor molecules [5–7]. Furthermore, the use of a self-assembled organic monolayer on the metal surface is a well-documented coating technique [1–7]. In this process, the inhibitor molecules form a self-assembled film on the electrode surface.

These monolayers have become very attractive because of their ease of preparation and their flexible properties. Indeed, the possibility of inserting different functional groups

inside or at the end of these monolayers means that many surfaces with different mechanical, chemical, and physical properties can be constructed. Previous work includes studies that led to research into SAMs by Langmuir and Burr Blodgett, who observed the physical adsorption of organic molecules onto the surface of metals. Plants possess numerous fascinating properties due to the presence of various organic families that are both renewable and abundant [5]. The molecules of which they are composed, such as alkaloids and phenolic compounds, are widely used in the process of protecting metals [8–10].

Sargassum is accessible and available in large quantities depending on the season, and these brown algae could prove to be an important and promising source of organic molecules with inhibiting properties. Two species of algae in the *Sargassum* genus have been identified on the Martinique coast, namely *Sargassum fluitans III* and *Sargassum natans*. The use of corrosion inhibitors derived from *Sargassum* seaweed would open up a new way of adding value to *Sargassum*, while at the same time responding to a developing area of research that is the subject of numerous publications each year [11,12]. As the extract of *Sargassum fluitans III* has given significant inhibition results in previous work carried out in submerged environments [13,14], this species was chosen for this study.

In this study, we will investigate the protective effect of crude extracts from *Sargassum fluitans III* on zinc's surface through the SAMs process. The crude extracts will be tested in two marine atmospheres in Martinique with different characteristics: the atmosphere of Frégate est, rich in H_2S due to intense *Sargassum* strandings, and the atmosphere of Diamant, rich in chloride ions. The efficacy of the *Sargassum* extract will be assessed by measuring mass loss. The corrosion surfaces will be analyzed by FTIR and XRD. Electrochemical impedance spectroscopy was be used to define the elementary corrosion mechanisms.

2. Materials and Methods

2.1. Sample Preparation

The zinc samples studied were 99% pure. They measured 100 mm × 75 mm × 1 mm. Before any treatment, the samples were chemically stripped by immersion in a 10% sulfuric acid bath for a few seconds, and then mechanically polished with SiC up to grade 1200, rinsed with distilled water and ethanol, dried, and weighed to the nearest 10^{-4} g using an Adam Nimbus 210-001 microbalance.

After this step, the samples were immersed in a solution of crude extract of *Sargassum fluitans III* obtained by refluxing with a mixture of 50% ethanol and distilled water. The preparation protocol for this extract was described in a previous study by Lambert et al. [13]. The zinc samples were immersed for 8 h in the crude extract of *Sargassum fluitans III*. The samples were then exposed at the two selected sites on inclined racks at 45°, in accordance with the EN13523-19 standard [15], for 3 months. A triplicate of samples was exposed at each site, with or without coating.

2.2. Selection of Sites

Figure 1 shows the location of the two selected sites on a map of Martinique. The two selected sites are Frégate est and Diamant. The corrosion of zinc at these two sites has already been studied [4]. The two sites are subject to the same climate. The average monthly temperature and relative humidity are 27 °C and 74%, respectively. However, corrosion at these two sites differs due to their variable exposure to sargassum seaweed wash-ups. Indeed, previous studies have shown that the atmosphere in Frégate est is rich in H_2S due to significant sargassum wash-ups and their degradation, while the atmosphere in Diamant possesses all the characteristics of a typical marine atmosphere. The concentrations of H_2S and chloride ions have been measured and reported in previous studies [4,16]. The elevated concentrations during the exposure periods are summarized in Table 1. Based on these data, two types of atmospheres are clearly identifiable: an atmosphere rich in H_2S (Frégate est) and an atmosphere rich in Cl^- ions (Diamant).

Figure 1. Position of the different sites on the map of Martinique.

Table 1. Average concentrations of H_2S and Cl^- ions at the different sites for 3 months.

Sites	H_2S (ppb)	Cl^- Deposited ($mg \cdot m^{-2} \cdot day^{-1}$)
Diamant	5	470
Frégate est	2590	56

2.3. Gravimetric Analysis

The zinc samples were chemically treated according to standard NF EN 8407 to remove corrosion products [17]. Before any chemical treatment, the surfaces of the samples were lightly brushed mechanically to remove corrosion products that did not adhere well. The samples were treated in a solution of ammonium chloride (100 g in 900 mL of distilled water) at 70 °C for 2 to 20 min. The treatment was carried out in an ultrasonic bath to optimize the process. The samples were then rinsed with distilled water and ethanol, air-dried, and weighed to determine the mass loss. This process was repeated several times for each sample until a mass plateau was reached. The experiment was performed on triplicate samples, and the average corrosion rate was calculated.

2.4. Electrochemical Measurements

The electrochemical measurements were carried out using a three-electrode set-up connected to a Bio-Logic VMP3 potentiostat (Orlando, FL, USA). The previously exposed zinc plate was used as the working electrode. A saturated $Hg/Hg_2Cl_2/KCl$ calomel electrode was used as the reference electrode, and a platinum electrode as the counter-electrode. For each test, the open circuit potential (OCP) was measured as a function of time. Once the medium was stable, the value recorded corresponded to the corrosion potential (E_{corr}) of the working electrode used. Electrochemical impedance spectroscopy (EIS) measurements were carried out using signals with an amplitude of ±2.5 mV at a scanning frequency of between 100 kHz and 10 mHz. For each of the concentrations tested, the above experiments were carried out in duplicate, and all the data collected were analyzed using EC-Lab V11.43 software.

2.5. FTIR and XRD Analysis

The zinc corrosion products were identified by XRD using Panalytical Empyrean apparatus (Malvern, UK) with CuKα radiation (1.5408 Å) according to the procedures described in previous publications [4,16,18].

The FTIR spectra of the samples were recorded with an ALPHA II compact FTIR spectrometer, in a wavenumber range from 400 to 4000 cm^{-1}, using the attenuated total reflection (ATR) mode (64 scans and a resolution of 4 cm^{-1}). The attenuated total reflection (ATR) set-up is specific to the study of layers deposited on a substrate.

3. Results and Discussion

3.1. FTIR Spectroscopy Analysis

FTIR spectroscopy analysis of a zinc surface modified by the SAMs process after 6 h of self-assembly in a 10^{-2} M solution of extract was carried out to determine the structural characteristics of the SAMs. The FTIR spectrum of the extract and the extract/SAMs spectrum are presented in Figure 2. In a previous study [13], we showed that the extract contains several compound families, such as coumarins, anthocyanins, quinones, flavonoids, saponins, tannins, and triterpenes. We were able to demonstrated this in our previous study because most of the IR bands observed were characteristic of the presence of the different families present in the total extract, namely 3347–3320 cm^{-1}, intermolecular O–H elongation; 2981–2881 cm^{-1}, symmetrical C–H elongation in an aromatic ring; 1646–1644 cm^{-1}, phenyl-type C=C elongation; 1407–1379 cm^{-1}, phenolic ring stretching from in-plane OH deformation; 1087–1043 cm^{-1}, cyclic ether C–O elongation; and 879–638 cm^{-1}, out-of-plane aromatic ring C-H deformation. Additionally, there was a band around 1650 cm^{-1}, characteristic of quinone derivatives. Compared to the crude sargassum extract, the extract/SAMs coatings exhibit a similar characteristic spectrum (Figure 2). However, a slight shift is generally observed for all absorption bands, indicating that an interaction between the extract and the zinc surface has taken place. This suggests that the organic coating, formed by SAMs, is primarily composed of neutral species of the extract molecules. The IR spectra show dependence on immersion time. The analysis of the IR spectra reveals the same peaks with different intensities, indicating that the adsorbed quantity depends on the immersion time.

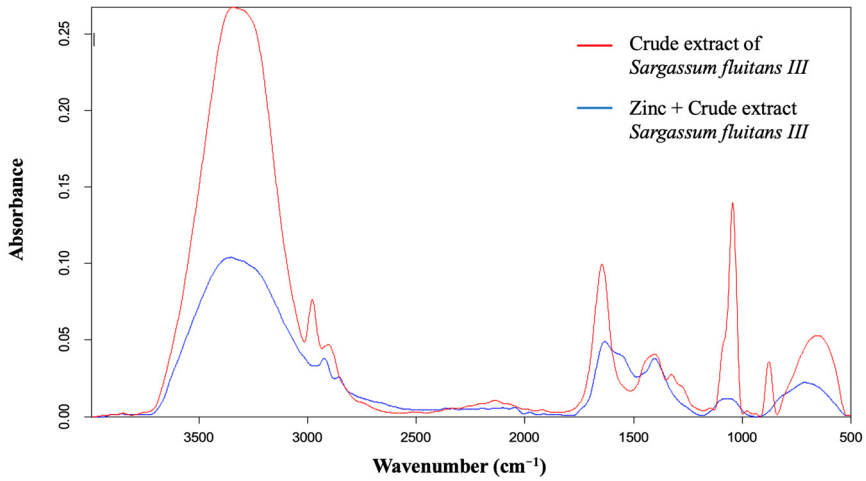

Figure 2. Infrared spectrum of crude sargassum extract and SAMs of extract on zinc surface.

3.2. Effect of Immersion Time on Film Formation

In this study, immersion time was recognized as a crucial factor for assessing the formation of the film, necessitating an evaluation of inhibition efficiency over an extended immersion time. Specifically, the investigation focused on the impact of immersion time ranging from 2 to 8 h on corrosion inhibition through EIS measurements. The self-assembled films developed in a solution containing ethanol and 200 mg/L of sargassum extract. This

concentration was chosen according to a previously published study [16] showing that at this concentration, maximum effectiveness is achieved.

The acquired Nyquist plot does not display a perfectly formed semicircle (Figure 3). To account for the depression of the semicircle caused by frequency dispersion in the experimental system, which can be attributed to factors such as surface inhomogeneity, roughness, electrode porosity, disorder, geometric irregularities, and others, it is necessary to replace the capacitor (C) with a constant phase element (CPE). This modification aims to compensate for the observed deviations in the Nyquist plot. The CPE is defined in the impedance representation as:

$$Z_{CPE} = \frac{1}{Q}(jw)^{-\alpha} \quad (1)$$

where Q is the CPE constant, ω is the angular frequency (in rad·s^{-1}), j^2 = -1 is the imaginary number and α is a CPE exponent.

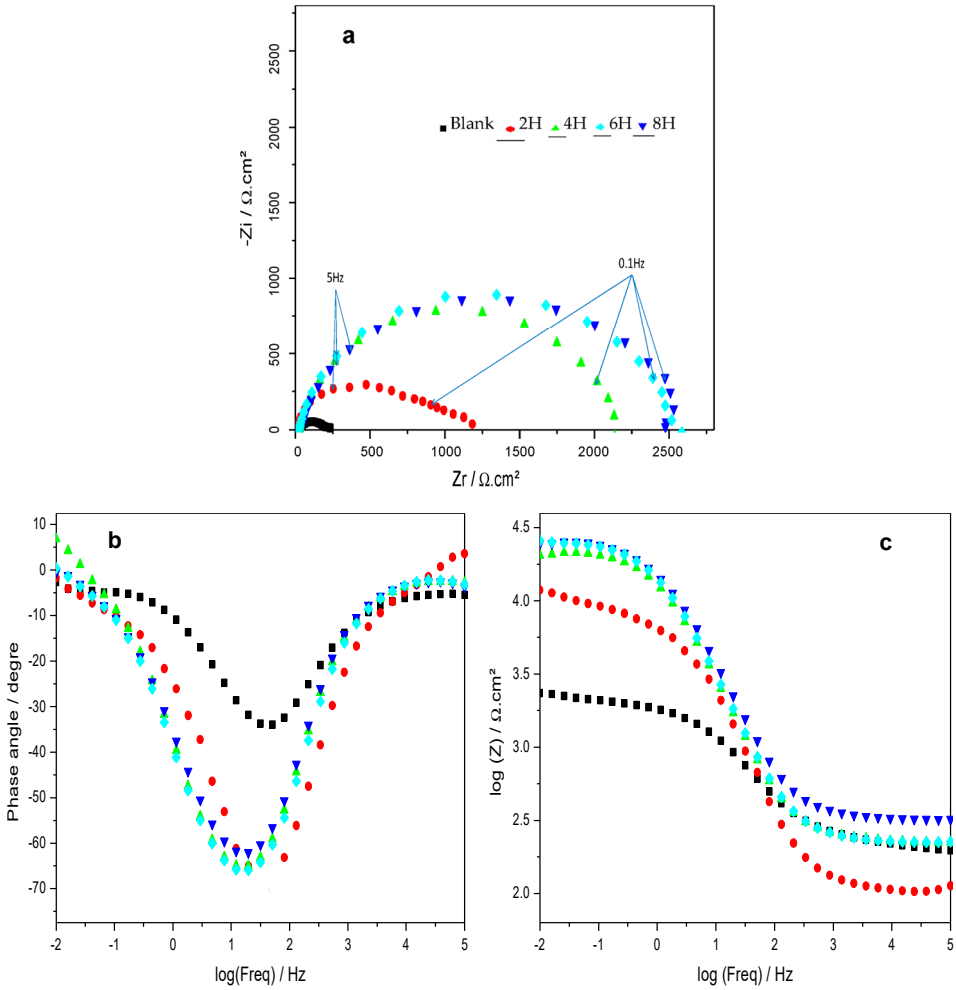

Figure 3. Nyquist (**a**) and Bode diagrams: phase (**b**) and impedance modulus (**c**) obtained in 3% NaCl at 25 °C for zinc surfaces without and with modification of sargassum extract/SAMs for different times of self-assembly.

These plots indicate a single capacitive loop in the shape of a semicircle, suggesting that the corrosion reaction of zinc in the NaCl solution is controlled by a charge transfer process [19,20]. The impedance is significantly enhanced in the extract/SAM-modified zinc electrodes compared to the bare electrode. Generally, a larger capacitive loop indicates better anticorrosion protection performance [21].

The Nyquist plots of modified electrodes share comparable forms but significantly differ in scale, with the largest semicircle linked to 6–8 h of self-assembly. The overall impedance modulus at 0.01 Hz (|Z|0.01 Hz) measures 3.37 Ω cm^2 for unmodified zinc and increases to 4.175, 4.26, 4.41, and 4.45 Ω cm^2 for 2 h, 4 h, 6 h, and 8 h of self-assembly, respectively (as depicted in Figure 1). Additionally, the maximum phase angles (αmax) for the unmodified zinc and modified extract/SAMs samples are −35.2°, −64.4°, −65.1°, −68.3°, and −68.3°, sequentially, illustrating enhanced shielding properties with extended self-assembly time, showing the characteristics of an electrode covered with a uniform and protective layer [22–24].

Such behavior may be due to the development of an adsorbed layer in the early stages of self-assembly, which, however, lacks organization and density and may have defects. Research has indicated that electrons can pass through SAMs even when devoid of defects, yet SAMs commonly include molecular imperfections. Zamborini and Crooks reported a study investigating the corrosion passivation properties of aromatic- and linear-chain organomercaptan SAMs on copper electro-oxidation in aqueous $HClO_4$ using spectroscopic, voltametric, and electrochemical scanning tunneling microscopic (ECSTM) techniques. They suggested a corrosion mechanism for electrodes re-covered with SAMs bearing defects [25]. Corrosive ions like chlorides can infiltrate SAMs through unoccupied defect sites, establishing contact with the bare metal surface, and subsequently causing corrosion of the metal substrate, ultimately resulting in SAMs' destruction. Laibinis et al. reported that self-assembled monolayers (SAMs) derived from the adsorption of n-alkanethiols onto copper surfaces slow down the oxidation of the copper surface by interacting with atmospheric oxygen. They suggested a corrosion mechanism for electrodes re-covered with SAMs bearing defects [26].

Brzoska et al. observed that increasing the self-assembly time leads to greater molecular adsorption onto the surface, subsequently causing the monolayer to become denser and more compact due to molecular rearrangement [27]. This observation suggests that sargassum extract could serve as an effective corrosion inhibitor in surface modification through the SAMs process, forming a dense film on the zinc surface and thereby counteracting metal corrosion. The thickness of the SAMs was not measured in this study, but according to the literature, it is expected to be between 1 and 10 nm. Previous studies on SAMs formed to protect iron from corrosion showed that the thickness of SAMs ranged from 2 to 10 nm [28]. Other works revealed that SAMs form as a thin film through spontaneous chemisorption, and the average thickness of SAMs is typically between 1 and 3 nm [29].

The experimentally obtained impedance data were modeled by the equivalent electrical circuit (EEC) shown in the Figure 4, with low values of the error factor χ^2 confirming the use of the proposed EEC. The electrochemical parameters of bare and SAM-modified zinc were determined by parametric fitting of the Bode and Nyquist diagrams and are presented in Table 2.

Table 2. Parameters deduced from EIS data obtained in 3% NaCl at 25 °C for zinc surfaces without and with modification of sargassum extract/SAMs for different times of self-assembly.

	Immersion Time	R_t (Ω·cm^2)	10^{-4} Q (Ω^{-1}·cm^{-2}·s^{α})	α	χ^2	θ (%)
Without SAMs	Blank	251 ± 2.08	2.4 ± 0.08	0.752 ± 0.002	2.8×10^{-3}	-
With SAMs	2H	1476 ± 4.21	1.87 ± 0.03	0.792 ± 0.011	2.3×10^{-3}	0.83
	4H	2243 ± 3.75	1.57 ± 0.01	0.803 ± 0.002	1.5×10^{-3}	0.89
	6H	2454 ± 1.73	1.17 ± 0.06	0.815 ± 0.006	1.9×10^{-3}	0.90
	8H	2517 ± 5.43	0.92 ± 0.02	0.831 ± 0.008	3.2×10^{-3}	0.90

Figure 4. Equivalent electrical circuit (EEC) of the metal/NaCl interface, used to fit impedance diagrams.

Upon assessing these findings, it is evident that the Rt values for modified substrates are considerably higher than those for bare zinc and escalate as self-assembly time extends. This implies that the extract/SAMs significantly improve zinc's corrosion resistance in a corrosive 3% NaCl solution. The n factor, reflecting electrode roughness and physical-chemical heterogeneity, indicates increased values with greater self-assembly time. This suggests an enhanced capacity for creating a dense film due to the progressive adsorption of more molecules on the surface. This behavior has been documented in empirical research, as reported in [30]. The investigation also revealed that the surface coverage, (θ), derived from the charge transfer resistance using Equation (1), increased during immersion for time frames between 2 and 6 h, while maintaining consistency for more extended intervals. This outcome supports the two-phase categorization of the self-assembled formation process: a quick adsorption stage followed by slowed rearrangement. Assuming the saturated adsorption time to be approximately 8 h, subsequent experimental tests were designed using this time immersion.

$$(1 - \theta) = \frac{\mathrm{Rt}^{\circ}}{\mathrm{Rt}^{\mathrm{SAMs}}} \quad (2)$$

where Rt° and $\mathrm{Rt}^{\mathrm{SAMs}}$ are the charge transfer resistance of the bare zinc electrode and film-covered electrode.

3.3. Evaluation of Zinc Thickness Loss

Mass loss measurements were used to assess the corrosion kinetics of the samples exposed with and without the crude extract coating of *Sargassum fluitans III* at the studied sites. To better visualize the damage, mass loss was converted into thickness loss (ε) using Equation (3):

$$\varepsilon = \frac{10 \times \Delta m}{Sd} \quad (3)$$

where ε is expressed in μm; Δm is the mass lost (in grams); d is the density of the zinc (7.13 g/cm^3); and S is the surface area of the zinc (in cm^2).

Table 3 presents the average thickness losses of the zinc samples exposed at the two sites for 3 months. The thickness losses observed in Diamant and Frégate est, with and without the coating, are, respectively, 1.56 μm, 4 μm, 4.25 μm, and 11.25 μm. The thickness losses are greater in Frégate est. This is consistent with the corrosive aggressiveness of this atmosphere due to its high concentration of H_2S derived from the degradation of sargassum seaweed [4,16]. Corrosion in Diamant is exclusively associated with an atmosphere abundant in sea spray laden with chloride ions. Furthermore, the presence of the coating on the zinc surface halved the thickness losses in both cases. These findings suggest that *Sargassum* extracts have a protective effect on zinc against corrosion independent of the corrosive environment. This indicates that the corrosion inhibition properties of *Sargassum* extracts extend beyond specific environmental conditions. The atmospheric environments at Frégate est and Le Diamant are classified as extremely corrosive, exceeding the upper limit of category CX, according to the NF EN ISO 9223 standard [31]. However, the presence of *Sargassum fluitans III* extract reduced the corrosiveness level of the atmosphere in Diamant from class CX to class C5.

Table 3. Loss of zinc thickness after two months of exposure. For each site, several samples were exposed. Values correspond to averages of triplicate batches exposed.

Sites	Surface State	Loss of Thickness (μm)
Diamant	Without coating	4.00 ± 0.01
	With coating	1.56 ± 0.02
Frégate est	Without coating	11.00 ± 0.01
	With coating	4.25 ± 0.01

3.4. Electrochemical Results

The study conducted through gravimetry offers limited insight into the mechanisms that drive corrosion. The Nyquist diagrams of zinc samples, with and without SAMs treatment, exposed to the atmosphere at Frégate est and Diamant for three months are shown in Figure 5. The Nyquist plots do not form perfect semicircles, owing to interfacial impedance frequency dispersion attributed to the zinc electrode surface's heterogeneity. These plots exhibit a single capacitive loop in the form of a semicircle, suggesting that zinc corrosion in the NaCl solution is controlled by a charge transfer process. The *Sargassum* extract-modified zinc electrode impedance is considerably increased compared to the unmodified bare electrode for the extract/SAM-treated zinc electrodes.

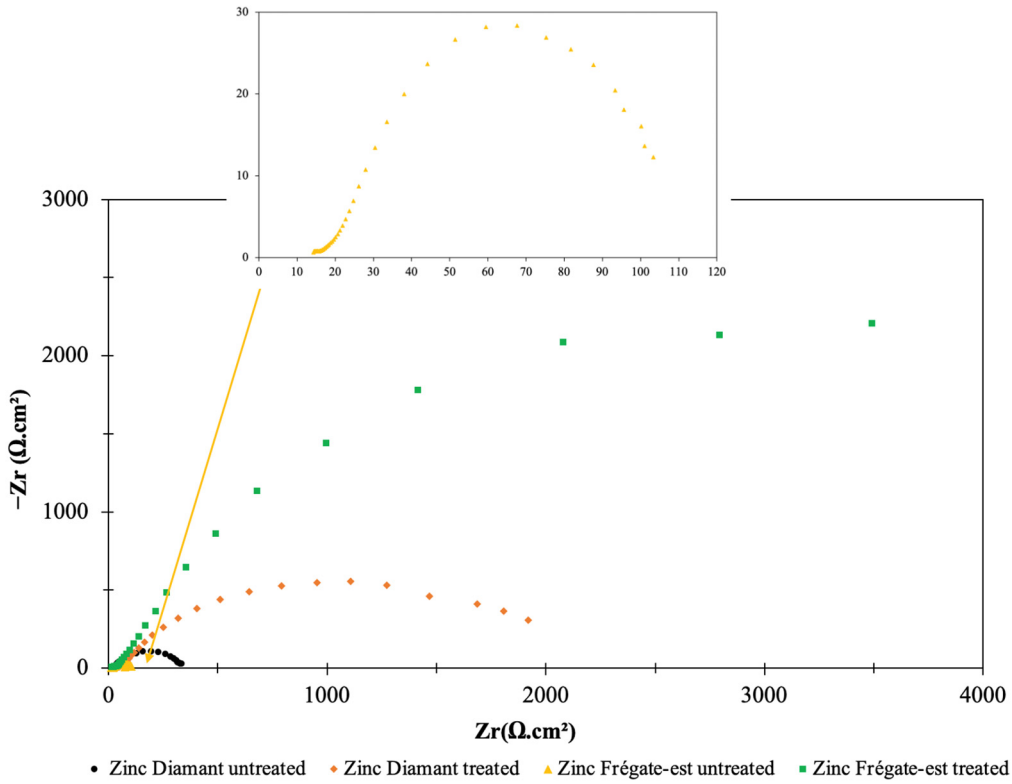

Figure 5. Nyquist plots in NaCl obtained for samples of zinc, without and with modification of Sargassum extract/SAMs, exposed in Diamant and Frégate est for three months.

Indeed, in electrochemical impedance spectroscopy (EIS), the size of the capacitive loop is indicative of the anticorrosion protection performance of the material in question. Generally, a larger capacitive loop suggests superior corrosion resistance. In this case, the extract/SAM-modified zinc electrodes demonstrate increased capacitive loop sizes compared to the bare electrode, indicating enhanced anticorrosion protection due to the presence of the self-assembled extract/SAMs. This observation highlights the potential of using sargassum extract in the SAMs process to inhibit atmospheric corrosion and

improve the durability of zinc-based materials, providing a valuable contribution to the advancement of material science research.

3.5. XRD Results

To supplement the results obtained by gravimetry and to better understand the corrosion mechanisms, the corrosion surfaces of zinc were analyzed by XRD. Figure 6 shows the diffractograms obtained after exposing zinc samples without (a, c) and with (b, d) the coating based on raw extracts of *Sargassum fluitans III* for 3 months in Diamant (a, b) and Frégate est (c, d).

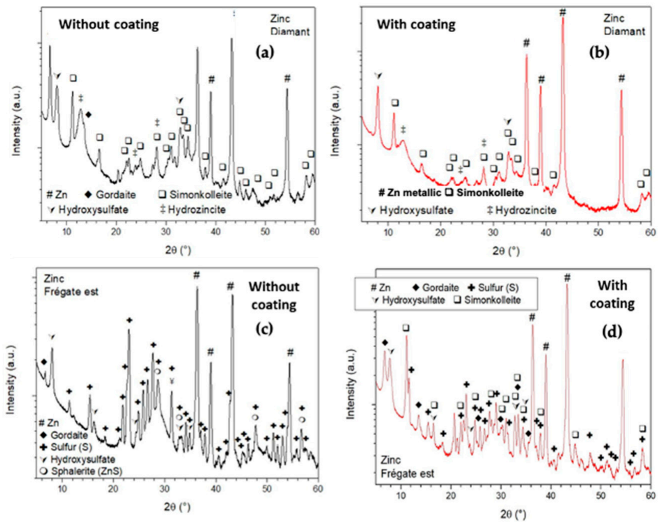

Figure 6. XRD diffractograms of zinc samples exposed for 3 months in Diamant and Frégate est, with (**b**,**d**) and without (**a**,**c**) coating based on crude extracts of *Sargassum fluitans III* algae.

In Diamant, the surfaces of the uncoated zinc show that simonkolleite ($Zn_5(OH)_8Cl_2{\cdot}H_2O$) is the main corrosion product (Figure 6a). Additionally, peaks corresponding to gordaite ($NaZn_4(SO_4)$ $(OH)_6Cl{\cdot}6H_2O$), hydroxysulfates ($Zn_4SO_4(OH)_6{\cdot}4H_2O$), and hydrozincite ($Zn_5(CO_3)_2(OH)_6$) are present at lower intensities. The intense peaks associated with metallic zinc indicate a thin corrosion layer. These zinc corrosion products are those found naturally in the atmosphere [32–35]. Simonkolleite is formed in marine atmospheres through the interaction between chloride ions and zinc oxide (ZnO) resulting from the dehydration of zinc hydroxide ($Zn(OH)_2$) (Equation (5)). This last compound is the precursor to zinc corrosion and is obtained through the electrochemical oxidation of zinc in the electrolytic layer, as described in Equation (4) [36].

$$Zn + \frac{1}{2}O_2 + H_2O \rightarrow Zn(OH)_2 \rightarrow ZnO \quad (4)$$

$$Zn(OH)_2 + 2Zn^{2+} + 6OH^- + 2Cl^- + H_2O \rightarrow Zn_5(OH)_8Cl_2{\cdot}H_2O \quad (5)$$

Hydrozincite is formed through the dissolution of CO_2 present in the atmosphere into carbonates ions. According to H. Tolosa [37], these react spontaneously with Zn^{2+} ions according to Equation (6). Hydrozincite is the corrosion product formed initially on zinc in a high-pH marine atmosphere, and dissolves easily under the action of chloride ions, SO_2, and/or H_2S.

$$5Zn^{2+} + 6OH^- + 2CO_3^{2-} + H_2O \rightarrow Zn_5(CO_3)_2(OH)_6 \quad (6)$$

The traces of hydroxysulphate observed on the diffractograms are linked to the presence of $SO_4{}^{2-}$ resulting from the oxidation of H_2S (present in trace form in the Diamant

atmosphere) by the oxygen dissolved in the electrolytic layer. Hydroxysulphate is formed from ZnO according to Equation (7).

$$3ZnO + Zn^{2+} + SO_4^{2-} + (3 + n)H_2O \rightarrow Zn_4SO_4(OH)_6 \cdot nH_2O \quad (7)$$

Gordaïte is the most thermodynamically stable corrosion product. It results from the progressive conversion of simonkolleite due to the high concentration of deposited salt and the surface acidity caused by the dissolution of sulfur gasses. This transformation occurs as indicated in Equation (8).

$$4Zn_4(OH)_8Cl_2 \cdot H_2O + 5Na + SO_4^{2-} + 24H_2O \rightarrow 5NaZn_4SO_4(OH)_6Cl \cdot 6H_2O + 3Cl^- + 8H^+ \quad (8)$$

The corrosion surfaces of zinc exposed with the coating show a composition similar to those without the coating (Figure 6b). Only gordaite is not identified on the surface. The absence of this product may indicate less advanced corrosion. This observation reinforces the results obtained by gravimetry, indicating a decrease in corrosion rate for coated zinc surfaces. Indeed, in a previous study, Lambert et al. [13] demonstrated that crude extracts of *Sargassum fluitans III* algae contain various chemical families, including coumarins, anthocyanins, quinones, flavonoids, saponins, tannins, and triterpenes, which possess anti-corrosion properties. Moreover, *Sargassum fluitans III* extracts have already shown effectiveness in inhibiting corrosion on steel in acidic environments exceeding 90%. The interaction between zinc and these chemical species, forming a barrier against corrosive agents, could explain the slowdown in corrosion.

The diffractograms of the zinc surface exposed to Frégate est for 3 months without and with the coating are shown in Figure 6c,d, respectively. Uncoated (Figure 6c), the predominant structure identified is attributed to elemental sulfur. This result is explained by the high concentrations of H_2S reported at this site, as previously demonstrated by M. Said Ahmed et al. [16]. Several hypotheses have been proposed to explain the process of elemental sulfur formation [30,32–35]. However, the most plausible in our case involves the oxidation of H_2S by oxygen, as shown in Equation (9) [38,39].

$$8\ H_2S + 4O_2 \rightarrow S_8 + 8H_2O \quad (9)$$

Figure 6c also shows the presence of sphalerite (ZnS). Its formation results from the interaction between H_2S and zinc metallic, as described in Equation (10) [40]. Other authors suggest that ZnS could result from the interaction between zinc and elemental sulfur (Equation (11)) [38]. The surface of the zinc exposed with the coating (Figure 6d) has a composition similar to that of the uncoated surface. Only ZnS is not identified. The absence of ZnS confirms the hypothesis of the formation of a physical barrier by the chemical species present in the extract of *Sargassum fluitans III* between the zinc and the corrosive environment. This barrier appears to limit the dissolution of zinc, and this would explain the low corrosion rates observed.

$$Zn + H_2S \rightarrow ZnS + H_2 \quad (10)$$

$$8Zn + S_8 \rightarrow 8ZnS \quad (11)$$

4. Conclusions

A SAM based on *Sargassum* extract was successfully formed on a zinc surface using a simple synthesis approach known as the SAMs process. Based on the investigation carried out, the following key findings were concluded:

- IR analysis confirmed the presence of *Sargassum fluitans III* extract adsorbed onto the metal surface, supporting successful formation of the extract-based self-assembled monolayer through the SAMs process.

- A study of the zinc immersion time within the extract revealed a saturation point between 6 and 8 h of contact, indicating an optimized time frame for material modification and potential improvement in the coating efficiency.
- The mass loss measurements, obtained after three months of exposure in two different sites, showed a significant reduction in the loss of zinc thickness after treatment with the extract-based coating. The formation of SAMs demonstrated a substantial reduction in the corrosion effects caused by the protective film, which improved the performance and durability of the zinc.
- These protective properties were validated through electrochemistry by comparing the impedance curves of zinc samples both with and without the coating. The curves for coated zinc showed enhanced impedance, implying a more effective shield against corrosion compared to the uncoated material.
- DRX analysis confirmed the absence of ZnS on the zinc surface. As ZnS is generally associated with corrosion in H_2S-rich environments, this indicates that the *Sargassum fluitans III extract*-based coating used in this study possesses a protective effect under such conditions.

Author Contributions: Conceptualization, M.L.; methodology, P.L., M.S.-A., M.L., B.L. and S.R.; software, P.L. and M.S.-A.; validation, M.L.; formal analysis, M.S.-A., M.L., B.L., S.R. and P.L.; investigation, P.L., M.S.-A., M.L., B.L. and S.R.; resources, M.L.; data curation, P.L., M.S.-A. and M.L.; writing—original draft preparation, P.L., M.S.-A. and M.L.; writing—review and editing, P.L., M.S.-A. and M.L.; visualization, M.S.-A. and M.L.; supervision, M.S.-A. and M.L.; project administration, M.L.; funding acquisition, M.L. All authors have read and agreed to the published version of the manuscript.

Funding: This research was funded by the Territorial Authority of Martinique (CTM).

Data Availability Statement: The raw data supporting the conclusions of this article will be made available by the authors on request.

Conflicts of Interest: The authors declare no conflicts of interest.

References

1. Morcillo, M.; Chico, B.; Fuente, D.; Simancas, J. Looking Back on Contributions in the Field of Atmospheric Corrosion Offered by the MICAT Ibero-American Testing Network. *Int. J. Corros.* **2012**, *2012*, 824365. [CrossRef]
2. Fuentes, M.; de la Fuente, D.; Chico, B.; Llorente, I.; Jiménez, J.A.; Morcillo, M. Atmospheric Corrosion of Zinc in Coastal Atmospheres. *Mater. Corros.* **2019**, *70*, 1005–1015. [CrossRef]
3. Thierry, D.; LeBozec, N.; Le Gac, A.; Persson, D. Long-Term Atmospheric Corrosion Rates of Hot Dip Galvanised Steel and Zinc-Aluminium-Magnesium Coated Steel. *Mater. Corros.* **2019**, *70*, 2220–2227. [CrossRef]
4. Ahmed, M.S.; Lebrini, M.; Pellé, J.; Rioual, S.; Amintas, O.; Boulanger, C.; Lescop, B.; Roos, C. Study of Atmospheric Corrosion of Zinc in a Tropical Marine Environment Rich in H2S, Resulting from the Decomposition of Sargassum Algae. *Mater. Corros.* **2024**. [CrossRef]
5. Faustin, M.; Lebrini, M.; Robert, F.; Roos, C. Corrosion Studies of C38 Steel by Alkaloids Extract of a Tropical Plant Type. *Int. J. Electrochem. Sci.* **2011**, *6*, 4095–4113. [CrossRef]
6. Lebrini, M.; Suedile, F.; Salvin, P.; Roos, C.; Zarrouk, A.; Jama, C.; Bentiss, F. Bagassa Guianensis Ethanol Extract Used as Sustainable Eco-Friendly Inhibitor for Zinc Corrosion in 3% NaCl: Electrochemical and XPS Studies. *Surf. Interfaces* **2020**, *20*, 100588. [CrossRef]
7. Suedile, F.; Robert, F.; Roos, C.; Lebrini, M. Corrosion Inhibition of Zinc by Mansoa Alliacea Plant Extract in Sodium Chloride Media: Extraction, Characterization and Electrochemical Studies. *Electrochim. Acta* **2014**, *133*, 631–638. [CrossRef]
8. Cáceres, L.; Frez, Y.; Galleguillos, F.; Soliz, A.; Gómez-Silva, B.; Borquez, J. Aqueous Dried Extract of Skytanthus Acutus Meyen as Corrosion Inhibitor of Carbon Steel in Neutral Chloride Solutions. *Metals* **2021**, *11*, 1992. [CrossRef]
9. Ortega Ramirez, A.T.; Barrantes, L.; Casallas Martin, B.D.; Cortés Salazar, N. Application of Green Inhibitors for Corrosion Control in Metals. Review. *Dyna* **2021**, *88*, 160–168. [CrossRef]
10. Shang, Z.; Zhu, J. Overview on Plant Extracts as Green Corrosion Inhibitors in the Oil and Gas Fields. *J. Mater. Res. Technol.* **2021**, *15*, 5078–5094. [CrossRef]
11. Suedile, F. Extraction, Caractérisation et Etude Electrochimique de Molécules Actives Issues de la Forêt Amazonienne pour la Protection du Zinc Contre la Corrosion., des Antilles et de la Guyane. 2014. Available online: https://theses.fr/2014AGUY0745 (accessed on 1 August 2024).

12. Lebrini, M.; Robert, F.; Lecante, A.; Roos, C. Corrosion Inhibition of C38 Steel in 1 M Hydrochloric Acid Medium by Alkaloids Extract from Oxandra Asbeckii Plant. *Corros. Sci.* **2011**, *53*, 687–695. [CrossRef]
13. Lambert, P.; Said-Ahmed, M.; Jama, C.; Lebrini, M. Molecules from Sargassum Algae as Green Inhibitor for C38 in HCl Medium: Extraction, Characterization and Electrochemical Study. *Coatings* **2023**, *13*, 2076. [CrossRef]
14. Vazquez-Delfin, E.F.; Velazquez, V.A.; Ramirez, D.R. *SargaZoom*; Cinvestav Mérida: Mérida, Mexico, 2020.
15. *EN13523-19*; Coil Coated Metals—Test Methods—Part 19: Panel Design and Method of Atmospheric Exposure Testing. iTeh Standard Preview: Brussels, Belgium, 2019.
16. Ahmed, M.S.; Lebrini, M.; Lescop, B.; Pellé, J.; Rioual, S.; Amintas, O.; Boullanger, C.; Roos, C. Corrosion of Copper in a Tropical Marine Atmosphere Rich in H2S Resulting from the Decomposition of Sargassum Algae. *Metals* **2023**, *13*, 982. [CrossRef]
17. Landolt, D. *Corrosion et Chimie de Surfaces des Métaux (Traité des Matériaux, Volume 12) | Société Française de Métallurgie et de Matériaux*; Presses Polytechniques et Universitaires Romandes: Lausanne, Switzerland, 2003.
18. Said Ahmed, M.; Lescop, B.; Pellé, J.; Rioual, S.; Roos, C.; Lebrini, M. Corrosion of Carbon Steel in a Tropical Marine Environment Enhanced by H2S from Sargassum Seaweed Decomposition. *Metals* **2024**, *14*, 676. [CrossRef]
19. Popova, A.; Raicheva, S.; Sokolova, E.; Christov, M. Frequency Dispersion of the Interfacial Impedance at Mild Steel Corrosion in Acid Media in the Presence of Benzimidazole Derivatives. *Langmuir* **1996**, *12*, 2083–2089. [CrossRef]
20. Khaled, K.F.; Amin, M.A. Corrosion Monitoring of Mild Steel in Sulphuric Acid Solutions in Presence of Some Thiazole Derivatives–Molecular Dynamics, Chemical and Electrochemical Studies. *Corros. Sci.* **2009**, *51*, 1964–1975. [CrossRef]
21. Yu, Y.; Wang, Y.; Li, J.; Zhang, D.; Gao, L. In Situ Click-Assembling Monolayers on Copper Surface with Enhanced Corrosion Resistance. *Corros. Sci.* **2016**, *113*, 133–144. [CrossRef]
22. Schreiber, F. Structure and Growth of Self-Assembling Monolayers. *Prog. Surf. Sci.* **2000**, *65*, 151–257. [CrossRef]
23. Doneux, T. *Etude de La Monocouche Autoassemblée de 2-Mercaptobenzimidazole*; ULB: Bruxelles, Belgium, 2005.
24. Aramaki, K.; Shimura, T. Self-Assembled Monolayers of Carboxylate Ions on Passivated Iron for Preventing Passive Film Breakdown. *Corros. Sci.* **2004**, *46*, 313–328. [CrossRef]
25. Zamborini, F.P.; Campbell, J.K.; Crooks, R.M. Spectroscopic, Voltammetric, and Electrochemical Scanning Tunneling Microscopic Study of Underpotentially Deposited Cu Corrosion and Passivation with Self-Assembled Organomercaptan Monolayers. *Langmuir* **1998**, *14*, 640–647. [CrossRef]
26. Laibinis, P.E.; Whitesides, G.M. Self-Assembled Monolayers of n-Alkanethiolates on Copper Are Barrier Films That Protect the Metal against Oxidation by Air. *J. Am. Chem. Soc.* **1992**, *114*, 9022–9028. [CrossRef]
27. Brzoska, J.B.; Shahidzadeh, N.; Rondelez, F. Evidence of a Transition Temperature for the Optimum Deposition of Grafted Monolayer Coatings. *Nature* **1992**, *360*, 719–721. [CrossRef]
28. Beaux, J.; Caussé, N.; Esvan, J.; Delaunay, S.; Tireau, J.; Roy, M.; You, D.; Pébère, N. Impedance analysis of film-forming amines for the corrosion protection of a carbon steel. *Electrochim. Acta* **2018**, *283*, 699–707. [CrossRef]
29. Love, J.C.; Estroff, L.A.; Kriebel, J.K.; Nuzzo, R.G.; Whitesides, G.M. Self-Assembled Monolayers of Thiolates on Metals as a Form of Nanotechnology. *Chem. Rev.* **2005**, *105*, 1103–1170. [CrossRef] [PubMed]
30. Rao, B.A.; Reddy, M.N. Formation, Characterization and Corrosion Protection Efficiency of Self-Assembled 1-Octadecyl-1H-Imidazole Films on Copper for Corrosion Protection. *Arab. J. Chem.* **2017**, *10*, S3270–S3283.
31. *NF EN ISO 9223*; Corrosion des Métaux et Alliages—Corrosivité des Atmosphères—Classification, Détermination et Estimation. AFNOR: Paris, France, 2012.
32. Panchenko, Y.; Strekalov, P. Formation, Retention, and Waste of Products of Atmospheric Corrosion of Metals. 2. Kinetics of Corrosion and Waste. *Prot. Met.* **2005**, *41*, 557–567. [CrossRef]
33. Evans, U.R. Electrochemical Mechanism of Atmospheric Rusting. *Nature* **1965**, *206*, 980–982. [CrossRef]
34. Odnevall, I.; Leygraf, C. Formation of NaZn4Cl(OH)6SO4 · 6H2O in a Marine Atmosphere. *Corros. Sci.* **1993**, *34*, 1213–1229. [CrossRef]
35. Zhu, F.; Zhang, X.; Persson, D.; Thierry, D. In Situ Infrared Reflection Absorption Spectroscopy Studies of Confined Zinc Surfaces Exposed under Periodic Wet-Dry Conditions. *Electrochem. Solid-State Lett.* **2001**, *4*, B19–B22. [CrossRef]
36. Graedel, T.E. Corrosion Mechanisms for Zinc Exposed to the Atmosphere. *J. Electrochem. Soc.* **1989**, *136*, 193C. [CrossRef]
37. Tolosa, H. Etude Thermodynamique et Électrochimique de La Corrosion Atmosphérique Des Métaux à Usage Électrique. Ph.D. Thesis, Montpellier 2 University, Montpellier, France, 1992.
38. Sun, J.; Sun, C.; Zhang, G.; Li, X.; Zhao, W.; Jiang, T.; Liu, H.; Cheng, X.; Wang, Y. Effect of O_2 and H_2S Impurities on the Corrosion Behavior of X65 Steel in Water-Saturated Supercritical CO_2 System. *Corros. Sci.* **2016**, *107*, 31–40. [CrossRef]
39. Zhong, X.; Wang, Y.; Liang, J.; Chen, L.; Song, X. The Coupling Effect of O_2 and H_2S on the Corrosion of G20 Steel in a Simulating Environment of Flue Gas Injection in the Xinjiang Oil Field. *Materials* **2018**, *11*, 1635. [CrossRef] [PubMed]
40. Svensson, J.-E.; Johansson, L.-G. The Synergistic Effect of Hydrogen Sulfide and Nitrogen Dioxide on the Atmospheric Corrosion of Zinc. *J. Electrochem. Soc.* **1996**, *143*, 51. [CrossRef]